Environmental Pollution 252 (2019) 236–244

Contents lists available at ScienceDirect

Environmental Pollution

journal homepage: www.elsevier.com/locate/envpol

Enhancement of aqueous sulfate formation by the coexistence of NO_2/NH_3 under high ionic strengths in aerosol water★

Tianzeng Chen [a, b], Biwu Chu [a, b, c, *], Yanli Ge [a, b], Shuping Zhang [a, b], Qingxin Ma [a, b, c], Hong He [a, b, c], Shao-Meng Li [d]

[a] State Key Joint Laboratory of Environment Simulation and Pollution Control, Research Center for Eco-Environmental Sciences, Chinese Academy of Sciences, Beijing, 100085, China
[b] University of Chinese Academy of Sciences, Beijing, 100049, China
[c] Center for Excellence in Regional Atmospheric Environment, Institute of Urban Environment, Chinese Academy of Sciences, Xiamen, 361021, China
[d] Air Quality Research Division, Science and Technology Branch, Environment and Climate Change Canada, Toronto, M3H5T4, Canada

ARTICLE INFO

Article history:
Received 4 December 2018
Received in revised form
27 April 2019
Accepted 14 May 2019
Available online 23 May 2019

Keywords:
Sulfate
Aqueous-phase reaction
Aerosol water
Ionic strength
Ammonia

ABSTRACT

Current air quality models usually underestimate the concentration of ambient air sulfate, but the cause of this underestimation remains unclear. One reason for the underestimation is that the sulfate formation mechanism in the models is incomplete, and does not adequately consider the impact of the synergistic effects of high concentrations of multiple pollutants on sulfate formation. In this work, the roles of gaseous NO_2, NH_3 and solution ionic strength in the formation of sulfate in the aqueous phase were quantitatively investigated using a glass reactor and a 30 m^3 smog chamber, separately. The results showed that sulfate formation was enhanced to different degrees in the presence of gas-phase NO_2, NH_3 and their coexistence as solutes in both liquid solution and aerosol water. NH_3 enhances the aqueous oxidation of SO_2 by NO_2 mainly by accelerating the uptake of SO_2 through increased solubility. More importantly, we found that high ionic strength in aerosol water could significantly accelerate the aqueous oxidation of SO_2, resulting in unexpectedly high S(VI) formation rates. We estimate that under severe haze conditions, heterogeneous oxidation of SO_2 by NO_2 on aerosols may be much shorter than that through gas phase oxidation by OH, aided by high ionic strengths in aerosols. Considering the existence of complex air pollution conditions with high concentrations of NO_2, NH_3 and aerosol water, as expected in typical urban and suburban settings, the sulfate formation mechanisms revealed in the present work should be incorporated into air quality models to improve the prediction of sulfate concentrations.

1. Introduction

In recent years, along with rapid social and economic development, many areas in China have suffered from frequent haze events (Li et al., 2017b; Shen et al., 2015; Sun et al., 2006; Tan et al., 2009). Similar air quality issues are also encountered in other rapidly growing countries (Fedorova et al., 2013; Pachauri et al., 2013). During such events, high concentrations (up to 100 ppb) of SO_2, NO_x and NH_3 have been observed (Fu et al., 2015; Ianniello et al., 2010; Liu et al., 2013; Meng et al., 2011; Yang et al., 2009), and these gaseous precursors contributed to high concentrations of secondary species in $PM_{2.5}$ (Yang et al., 2011; Ye et al., 2011; Zhang et al., 2015b; Zhao et al., 2013). Sulfate (SO_4^{2-}) is a dominant component in $PM_{2.5}$ during these haze events and plays a significant role in haze formation under high relative humidity (RH) conditions (Guo et al., 2014; He et al., 2001; Pathak et al., 2009; Wang et al., 2005; Zhang et al., 2011).

Sulfate is primarily generated from the homogeneous oxidation of SO_2, mainly by OH radicals and Criegee intermediates (Mauldin Iii et al., 2012; Welz et al., 2012) in the gas phase, heterogeneous oxidation of SO_2 on particle surfaces (He et al., 2014; Liu et al., 2012; Ma et al., 2008), and aqueous oxidation of dissolved S(IV) (the sum of $SO_2 \cdot H_2O$, HSO_3^-, and SO_3^{2-}) by dissolved oxidants (e.g., H_2O_2, O_3, NO_2) and transition metals (e.g., Fe(III), Mn(II)) in cloud/fog droplets (Hung and Hoffmann, 2015; Li et al., 2017a; Quan et al., 2015; Seinfeld and Pandis, 2016; Xue et al., 2016). Both OH oxidation in

★ This paper has been recommended for acceptance by Dr. Sarah Harmon.

* Corresponding author. State Key Joint Laboratory of Environment Simulation and Pollution Control, Research Center for Eco-Environmental Sciences, Chinese Academy of Sciences, Beijing, 100085, China.
E-mail address: bwchu@rcees.ac.cn (B. Chu).

https://doi.org/10.1016/j.envpol.2019.05.119
0269-7491/

the gas phase and most aqueous oxidation reactions have been included in the Weather Research and Forecasting-Community Multiscale Air Quality (WRF-CMAQ) model system and most other air quality models, but simulation results have usually underestimated sulfate concentrations, especially under heavy haze pollution conditions (Cheng et al., 2016). Previous studies have demonstrated qualitative mechanisms for rapid sulfate growth under complex pollution conditions (Cheng et al., 2016; He et al., 2014; Li et al., 2018; Liu et al., 2012; Ma et al., 2008; Wang et al., 2016; Yang et al., 2016). For example, sulfate formation can be promoted by the coexistence of NO_x on the surface of mineral oxides (He et al., 2014; Liu et al., 2012; Ma et al., 2008; Xie et al., 2015). Synergistic effects were found between NH_3 and SO_2 on typical mineral dust particles; NH_3 increases the surface alkalinity and leads to water film on the surface of mineral dust, which enhances SO_2 adsorption on the surface and increases its oxidization to sulfate (Yang et al., 2016). However, the aqueous-phase oxidation of S(IV) by NO_2 was ignored in the description of the mechanism because of the low solubility of NO_2 under typical atmospheric conditions.

Due to the large discrepancies in the model-predicted pH of fine particles (Cheng et al., 2016; Guo et al., 2017; Liu et al., 2017; Wang et al., 2018; Wang et al., 2016), which might result from differences in model assumptions and inputs in those related studies (Song et al., 2018), the importance of the NO_2 pathway for sulfate formation in the aqueous phase remains unresolved. The aqueous-phase oxidation pathway of S(IV) by NO_2 has recently been shown to be a key mechanism in the formation of sulfate under fog/cloud conditions with high NO_2 concentration levels (Cheng et al., 2016; Li et al., 2018; Wang et al., 2016). Wang et al. (2016) also indicated that the neutralization of NH_3 could enhance sulfate formation from the reaction of S(IV) with NO_2 under aerosol water or cloud conditions, implying that this reaction was greatly influenced by the pH values of the aqueous phase (Clifton et al., 1988; Huie, 1994; Nash, 1979; Spindler et al., 2003). Previous studies have shown that with increases in pH, the aqueous-phase equilibrium concentration of S(IV) increased, clearly caused by the increased solubility of SO_2 (McVay and Ervens, 2017; Seinfeld and Pandis, 2016). Meanwhile, the reaction rate constant of S(IV) oxidization by dissolved NO_2 also increased significantly (Littlejohn et al., 1993). Studies also found that the rate and efficiency of NO_2 absorption could be enhanced during the process of simultaneous removal of SO_2 and NO_2 gases in alkaline solutions (Hu et al., 2010; Kameoka and Pigford, 1977; Takeuchi et al., 1977). The increased absorption of both SO_2 and NO_2 in alkaline solutions further enhanced the oxidation of sulfite (Shen and Rochelle, 1998). However, quantitative estimation of the increased absorption and oxidation rates in the presence of NO_2 and NH_3, for inclusion in a mechanism in air quality models to predict the sulfate concentration, is still lacking. This is one of the main subjects of this study.

In addition, ionic species significantly affect the ionic strength of the reaction media and result in different reaction media for the aqueous oxidation of SO_2 in bulk solutions (cloud droplets, fog) and aerosol water. Previous experimental studies have indicated that the ionic strength (I) of solutions could lead to changes in the rate constants (k) (Herrmann et al., 2015) for reactions leading to sulfate formation in the aqueous phase, such as S(IV) oxidation by H_2O_2, O_3, and NO_2. Studies have shown that an increase in solution ionic strength could increase the rate of oxidation of S(IV) by O_3 (Maahs, 1983) and by H_2O_2 in aqueous solutions (Ali et al., 2014; Maaβ et al., 1999). However, with respect to the oxidation of S(IV) by NO_2, there has been no report on the relationship of k and I, except for some plausible estimation (Cheng et al., 2016). The effects of ionic strength may be crucial for evaluating the importance of the aqueous-phase reactions, and need further investigation.

Hence, studying the synergistic effects among SO_2, NO_x and NH_3 in sulfate formation is important to reveal the formation mechanisms of sulfate in aerosol water, especially during severe haze events with high levels of NO_x and NH_3. There is a need to evaluate the effects of the coexistence of NH_3 and high ionic strength on the solubility and aqueous-phase oxidation of S(IV) by NO_2 in different reaction environments. The present work was carried out to address this need and to determine the significance of these effects.

2. Experimental section

2.1. Simulation of aqueous-phase reaction in a glass reactor

Simulation of aqueous sulfate formation was carried out in a glass reactor as shown in Fig. S1 (Volume = 600 mL, see in Supporting Information (SI)). The specifications of the gases used are as follows: SO_2 (100 ppm in N_2, Beijing Huayuan), NO_2 (100 ppm in N_2, Beijing Huayuan), carrier gas N_2 (99.999% purity, Beijing Huayuan). 6 mL ultrapure water (18.2 MΩ, Millipore Milli-Q) or 0.02 wt% NH_3 solution (Sinopharm Chemical Reagent Co., Ltd, Guaranteed reagent) were firstly added at the bottom of the glass reactor. Then, steady concentrations of SO_2 or/and NO_2 carried by high purity N_2 were introduced into the glass reactor at a flow rate of 2.0 L min^{-1} with Peclet number ~580, which indicated that the gas phase species were not transported to the interface of flow tube, so a mixing tube was used (see Fig. S1A, marked in red) to make sure the reaction gases were evenly mixed. As the reaction gases (SO_2 or/and NO_2) swept over the liquid surface, they would dissolve in the water, and aqueous-phase reaction would occur. After flowing the reaction gas for 10 min, the reaction cell was purged with 2.0 L min^{-1} of high purity N_2 for 5 min. All the simulations were carried out under dark conditions and at constant temperature (~298 K). Four different reaction systems, namely SO_2, SO_2/NH_3(aq), SO_2/NO_2 and $SO_2/NO_2/NH_3$(aq) were designed, marked as GR-SO_2, GR-SO_2/NH_3(aq), GR-SO_2/NO_2 and GR-$SO_2/NO_2/NH_3$(aq), respectively. The concentrations of SO_2 or/and NO_2 were controlled at about 300 ppb and 300 ppb, which were monitored with an interval of 1 min by a SO_2 analyzer (Model 43i, Thermo Fisher Scientific, Inc. USA) and NO_x analyzer (Model 42i-TL, Thermo Fisher Scientific, Inc. USA), respectively. The detailed conditions of the experiments are listed in Table 1. Additional parallel experiments in oxalic acid solution (Table S1) were also conducted. For each system, the simulation was repeated three times to understand the distribution due to experimental error, and the relative standard deviation (RSD) was also calculated to be less than 5%.

After reaction, the liquid samples were transferred to 5 mL vials (PolyVials™, Thermo Scientific, Inc. USA). 1 wt % formaldehyde (Sigma-Aldrich, ACS reagent, 37 wt % in H_2O) was added in order to suppress sulfite oxidation and avoid overestimating sulfate (Kong et al., 2014). Then the samples were analyzed by ion chromatography (IC, Model DIONEX ICS-2100 and ICS-1100, Thermo Scientific, Inc. USA) to determine the concentrations of water-soluble ions (e.g., SO_4^{2-}, NO_3^-, NH_4^+) (SI, Section S1). Meanwhile, the pH of the solution at the end of the reaction was determined by a pH meter (FE28-Standard, Mettler-Toledo Instruments Co., Ltd).

2.2. Simulation of aqueous-phase reaction in the smog chamber

We also performed experiments by exposing oxalic acid seed aerosols to gaseous SO_2, SO_2/NH_3, SO_2/NO_2 and $SO_2/NO_2/NH_3$, respectively under dark and high relative humidity (RH = (98 ± 1.5) %) conditions in a 30 m^3 smog chamber (SI, Section S2), these four experimental systems were marked as SC-SO_2, SC-SO_2/NH_3, SC-SO_2/NO_2 and SC-$SO_2/NO_2/NH_3$, respectively. SO_2 and NO_x were also monitored using a SO_2 analyzer and a NO_x analyzer mentioned

Table 1
Experimental conditions in different reaction systems.

Exp.[a]	Gaseous SO_2 (ppb)	Gaseous NO_2 (ppb)	Gaseous NH_3 (ppb)[b]	Aqueous conditions
GR-SO_2	300	–	–	Ultrapure water
GR-SO_2/NO_2	310	312	–	Ultrapure water
GR-SO_2/NH_3(aq)	302	–	–	0.02 wt %NH_3 solution
GR-SO_2/NO_2/NH_3(aq)	300	310	–	0.02 wt %NH_3 solution
SC-SO_2	298	–	–	Aerosol water of oxalic acid (RH = (98 ± 1.5) %)
SC-SO_2/NO_2	288	307	–	Aerosol water of oxalic acid (RH = (98 ± 1.5) %)
SC-SO_2/NH_3	288	–	~300	Aerosol water of oxalic acid (RH = (98 ± 1.5) %)
SC-SO_2/NO_2/NH_3	284	317	~300	Aerosol water of oxalic acid (RH = (98 ± 1.5) %)

[a] GR represents the experiments performed in the glass reactor; SC represents the experiments performed in the 30 m^3 smog chamber.
[b] NH_3 concentration is estimated by the amount of NH_3 added and the volume of the smog chamber.

above. For the concentration of NH_3, it was estimated according to the amount of NH_3 introduced and the volume of the chamber reactor. Aerosol particle size distributions and number concentrations were measured using a custom-built Scanning Mobility Particle Sizer (SMPS, TSI) with a 5-min cycle, which consists of a differential mobility analyzer (DMA, 3080 Classifier, TSI, Inc., USA) coupled with a Condensation Particle Counter (CPC, 3776, TSI, Inc., USA). Also, the mass concentrations of sulfate, nitrate and ammonium were measured using a high-resolution time-of-flight aerosol mass spectrometer (HR-ToF-AMS, Aerodyne Research Inc. USA). The wall loss of pollutants were measured in several specialized experiments at the beginning and the end of chamber experimental study. The deposition rate of the pollutants in these experiments turned out to be quite similar. The wall loss rates of gaseous NO_2 and SO_2 were $(1.67 \pm 0.25) \times 10^{-4}$ and $(3.32 \pm 0.21) \times 10^{-4}$, respectively. The wall loss rate (k_{dep}) of particles was in accordance with $k_{dep} = 4.15 \times 10^{-7} \times D_p^{1.89} + 1.39 \times D_p^{-0.88}$ (D_p is the particle diameter (nm)), which is used to correct the wall loss of aerosol particles similarly as Takekawa et al. (2003). T and RH were monitored using a hydro-thermometer (Vaisala HMP110).

Prior to each experiment, the Teflon chamber was flushed with purified and dry zero air for about 24 h at a flow rate of 100 L min^{-1} until there was almost no residual NO_x, SO_2, or NH_3, and the particle number concentration was <10 cm^{-3}. Before the experiments, the Teflon chamber was humidified to the expected RH by passing purified air through ultra-pure water (18.2 MΩ, Millipore Milli-Q). Then the oxalic acid seed aerosols were injected into the Teflon chamber by atomizing 0.02 M oxalic acid solution and passed through a diffusion dryer before entering the chamber. These seeds would absorb water and even become deliquescent under high RH conditions (Peng et al., 2001), and formed a liquid reaction environment on their surface. SO_2, NO_2, and NH_3 were then injected into the chamber in purified dry zero air. The concentrations of the gases were continuously monitored at a measurement point in the reactor. The initial concentration of gaseous NH_3 was approximately 300 ppb, as shown in Table 1, and the concentrations of SO_2 and NO_2 were similar to those in the simulation carried out in the glass reactor.

At the end of the experiments, filter samples were collected onto 47 mm pure quartz filters (0.3 μm pore size, Staplex Air Sampler Division, USA) by use of a vacuum pump with a flow rate of 10 L min^{-1} during the first 6 h of the cleaning process. The sampling port for the filters was located in the middle of the south side, and the cleaning air inlet was located in the middle of the east side of the smog chamber. After that, the collected filter samples were extracted in 12 mL of ultra-pure water in an amber sample vial (Strg Vial Kit, Agilent Technologies, USA) by sonication (Ultrasonic Cleanser, KQ-300DE) for 30 min, and then samples were analyzed by the IC system as mentioned above for the concentration of water-soluble inorganic ions, including SO_4^{2-}, NO_3^- and NH_4^+. The trend of the SO_4^{2-} concentration of the filter samples determined by IC was consistent with the AMS results (Fig. S2).

2.3. Determination of reaction kinetics

In order to calculate the reaction kinetics of heterogeneous reactions, the mass transport in different media needs to be taken into account (Cheng et al., 2016). Considering the mass transport, a standard resistance model was adopted to describe the relationship between the aqueous-phase reaction rate and the overall reaction rate (Cheng et al., 2016; Seinfeld and Pandis, 2016):

$$\frac{1}{R_{aq}} = \frac{1}{R_{H,aq}} - \frac{1}{J_{aq,\mathrm{lim}}} \quad (1)$$

where R_{aq} is the aqueous-phase reaction rate, $R_{H,aq}$ is the overall reaction rate, and $J_{aq,lim}$ is the limiting mass transfer rate.

$R_{H,aq}$ could be derived by Eq. (2) using the experimental results:

$$R_{H,aq} = \frac{\Delta[SO_4^{2-}]}{\Delta t} \quad (2)$$

in which ΔSO_4^{2-} is the concentration of sulfate determined by IC or HR-ToF-AMS, and Δt is the reaction time.

Correspondingly, the aqueous-phase reaction rate R_{aq} could be estimated by Eq. (3):

$$R_{aq} = k[S(IV)][NO_2] \quad (3)$$

where k is the reaction rate coefficient of the oxidation reaction, $[S(IV)]$ and $[NO_2]$ are the concentrations of $S(IV)$ and NO_2 in the aqueous phase, respectively, and $[NO_2]$ was determined by Henry's law:

$$[NO_2] = p(NO_2) \cdot H^*(NO_2) \quad (4)$$

where $p(NO_2)$ and $H^*(NO_2)$ are the partial pressure of NO_2 in the gas phase and the effective Henry's constant with 1.00×10^{-2} M atm^{-1} at 298K, respectively.

Meanwhile, $J_{aq,lim}$ could be determined via Eq. (5) and Eq. (6) as follows:

$$J_{aq,\mathrm{lim}} = \min\{J_{aq}(SO_2), J_{aq}(NO_2)\} \quad (5)$$

$$J_{aq}(X) = k_{MT}(X) \cdot p(X) \cdot H^*(X) \quad (6)$$

in which X refers to SO_2 or NO_2, and $k_{MT}(X)$ is the mass transfer rate coefficient of species X, which could be calculated by Eq. (7):

$$k_{MT}(X) = \left(\frac{R_p^2}{3D_g} + \frac{4R_p}{3\alpha v}\right)^{-1} \quad (7)$$

where R_p is the aerosol radius, D_g is the gas-phase molecular diffusion coefficient, α is the mass accommodation coefficient of

species X on the aqueous surface, with 0.11 (Seinfeld and Pandis, 2016) and 2.00×10^{-4} (Jacob, 2000) for SO_2 and NO_2, respectively. v is the mean molecular speed of species X.

3. Results and discussion

3.1. Description of the reaction process in different reaction systems

A simplified conceptual model of sulfate (S(VI) species will be mainly SO_4^{2-} under the pH conditions in GR reactions, while SO_4^{2-} and HSO_4^- may both exist under the pH conditions in SC reactions in this study) formation in the aqueous phase as investigated in this study is shown in Fig. 1, which includes the solubility of SO_2 and NO_2 (process I and II) and aqueous-phase oxidation (process III). SO_4^{2-} formation was determined in both a glass reactor with a water solution and in a smog chamber with aerosol water associated with oxalic acid seed aerosols. The experimental conditions for the reactions in the glass reactor (GR) and reactions in the smog chamber (SC) are summarized in Table 1. In the experiments GR-SO_2 and GR-SO_2/NH_3(aq), dissolved SO_2 (mainly HSO_3^-) was oxidized by background oxidants in the water (e.g., dissolved oxygen), while in the experiments GR-SO_2/NO_2 and GR-SO_2/NO_2/NH_3(aq), dissolved NO_2 (i.e., NO_2^-) also contributed to the oxidation of dissolved SO_2. Similar processes occurred in the aerosol water of the oxalic acid seed aerosols. The presence of NH_3 (in solution or in the gas phase) is expected to increase the alkalinity of the aqueous phase and influence both SO_2/NO_2 solubility and the oxidation rate of HSO_3^- by NO_2^-, which could be generated in the fast hydrolytic disproportionation of NO_2 (Li et al., 2018).

3.2. The role of NO_2 for SO_4^{2-} formation in the aqueous-phase oxidation

Fig. 2A summarizes the SO42- concentrations resulting from reactions in the GR system. Ten minutes after the start of reaction in the experiment GR-SO_2, the concentration of SO_4^{2-}, which came from the oxidation of dissolved SO_2 (mainly HSO_3^-) by background oxidants in the solution, was 0.005 ± 0.002 μg mL^{-1}. In the experiment GR-SO_2/NO_2, the SO_4^{2-} generated was 0.041 ± 0.001 μg mL^{-1}, which was increased by a factor of about 8 compared to GR-SO_2, suggesting a significant contribution of NO_2 to the oxidation of SO_2 in the water solution. The apparent reaction rate constant for the aqueous-phase oxidation of dissolved S(IV) by NO_2(aq) was calculated to be $1.31 \times 10^6 \pm 2.86 \times 10^4$ M^{-1} s^{-1}. The rate constant reported by Lee and Schwartz (1983) was 1.40×10^5 M^{-1} s^{-1} when pH < 5.0 and 2.00×10^6 M^{-1} s^{-1} when pH > 5.8, while Clifton et al. (1988) calculated the rate constant to be 1.24×10^7 M^{-1} s^{-1} and 1.67×10^7 M^{-1} s^{-1} at pH of 5.3 and 8.7, respectively. In the present study, the pH of the solution was 4.1 at the end of the reaction. Considering the uncertainty in pH, our experimental results for the reactions in water solution using the glass reactor are in the range of results from previous studies (Clifton et al., 1988; Huie and Neta, 1986; Lee and Schwartz, 1983).

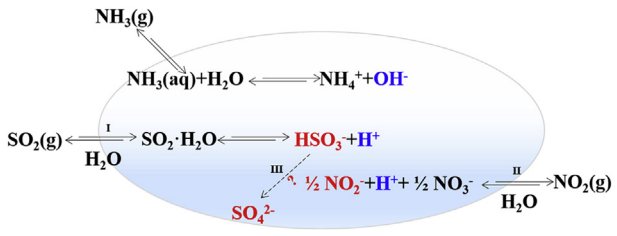

Fig. 1. A simplified conceptual model of SO_4^{2-} formation in the aqueous phase. Process I and II represent the dissolution of SO_2 and NO_2 into the aqueous phase, respectively, and process III represents SO_4^{2-} formation by NO_2 oxidation.

In the SC experiments using oxalic acid seed aerosols, there was also similar enhancement of the SO_4^{2-} formation from the oxidation of SO_2 by NO_2 (Fig. 2B). The time series of SO_2, NO_2, SO_4^{2-} and NO_3^- during each SC experiment were shown in Fig. S3. Normalizing SO_4^{2-} formation with the initial SO_2 concentration, SO_4^{2-} formation increased by 15.2% in the presence of NO_2. As shown in Fig. 3, the consumption rate of gaseous SO_2 (after correction for wall loss) was 5.26×10^{-4} min^{-1} in the experiment SC-SO_2/NO_2, which is higher than in SC-SO_2 (4.33×10^{-4} min^{-1}). Meanwhile, the size distributions for different SC experiments were also given in Fig. S4. Compared with SC-SO_2, the slightly larger particle size were observed in the SC-SO_2/NO_2 (~250 nm, Figs. S4A and S4B). Meanwhile, the reaction rate constant was calculated to be $1.56 \times 10^8 \pm 4.67 \times 10^6$ M^{-1} s^{-1} (Table 2), which is two orders of magnitude higher than that in the GR system. This was probably caused by the different reaction environments (e.g. the concentration of ionic species in the aqueous phase), and this influence will be discussed in detail later in this paper. Meanwhile, based on the concentrations of chemical species measured by HR-ToF-AMS, the molarity based pH (i.e., pH_c) of the aerosol water was estimated using the extended aerosol inorganics model (*E-AIM*, Model II) (Clegg et al., 1998; Wexler and Clegg, 2002; Jia et al., 2018). In the SC experiments, the gas-phase NH_3 concentration was estimated by considering the amount of NH_3 added and the volume of the smog chamber. Considering the uncertainty of the NH_3 concentration due to its strong stickiness with walls and other surfaces, and the presence of oxalic acid aerosols, which was not considered in the *E-AIM* model, the predicted pH of the aerosol by *E-AIM* model might have some uncertainty. In addition, recent studies have reported that organic compounds had an effect on pH (Guo et al., 2015; Jia et al., 2018; Pye et al., 2018). Therefore, the estimated pH_c was for reference only and was not used in the analysis of the results.

3.3. The role of NH_3 in SO_4^{2-} formation in the aqueous-phase reaction

Similarly, we studied the role of NH_3 in the aqueous-phase oxidation of SO_2. With the presence of NH_3 in the aqueous-phase reaction, the formation of SO_4^{2-} was enhanced to varying degrees (Fig. 2). In the GR system, 0.013 ± 0.006 μg mL^{-1} of SO_4^{2-} was formed in the experiment GR-SO_2/NH_3(aq), more than two times that in GR-SO_2. We attributed this increase in SO_4^{2-} formation to increased SO_2 dissolution due to the increase in the alkalinity of the reaction solution. In the experiment GR-SO_2/NO_2/NH_3(aq), SO_4^{2-} formation was promoted further by the presence of gaseous NO_2 and NH_3, and its concentration (0.22 ± 0.009 μg mL^{-1}) was about 44.0 times and 5.4 times that in the experiments GR-SO_2 and GR-SO_2/NO_2, respectively. These results are consistent with a previous study (Turšič et al., 2004) showing that the presence of NH_3 could promote SO_4^{2-} formation by a factor of 23 under aqueous droplet conditions. For the SC experiments, the presence of NH_3 in the experiment SC-SO_2/NH_3 enhanced the SO_4^{2-} formation by a factor of 4.4 compared to SC-SO_2 (1.19 μg m^{-3} vs 0.27 μg m^{-3}, respectively). The promotion of SO_4^{2-} formation due to NH_3 is more significant in the SC experiments than that in the GR experiments. One possible reason is that the presence of NH_3 in the SC experiments also increased the volume of aerosol water, while this effect did not exist in the GR experiments. This could be supported by the size distribution observed in SC-SO_2/NH_3 and SC-SO_2, in which the former had the larger particle size (Figs. S4A and S4C). Meanwhile, in another separate SC experiment, NH_3 was injected into the chamber with similar RH and quantity of oxalic acid seed aerosol. The seed aerosol volume rose 23% after the injection of NH_3 into the chamber (24.0 μm^3 cm^{-3} vs 29.6 μm^3 cm^{-3},

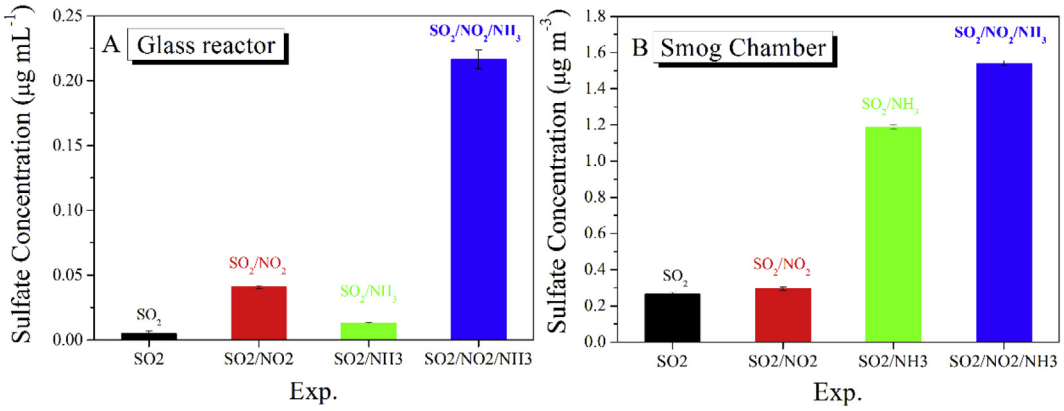

Fig. 2. The generated concentration of SO_4^{2-} (A) in GR under different experimental conditions, i.e., 300 ppb SO_2, 310 ppb SO_2/312 ppb NO_2, 302 ppb SO_2/NH_3(aq), and 300 ppb SO_2/310 ppb NO_2/NH_3(aq), and (B) in SC under analogous experimental conditions, i.e., 298 ppb SO_2, 288 ppb SO_2/307 ppb NO_2, 288 ppb SO_2/NH_3 (~300 ppb), and 284 ppb SO_2/317 ppb NO_2/NH_3 (~300 ppb). The error bars represent the standard deviations.

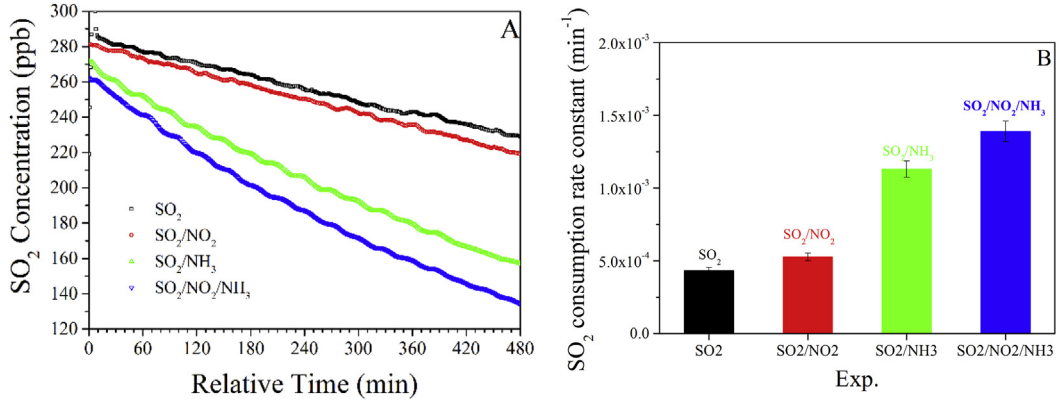

Fig. 3. (A) Time-resolved concentration and (B) consumption rate constant of SO_2 in the SC experiments under different conditions.

Table 2
Summary of reaction rate constants derived from different studies.

Exp.	Reaction rate constant (M^{-1} s^{-1})			
This study	GR-SO_2/NO_2	GR-$SO_2/NO_2/NH_3$(aq)	SC-SO_2/NO_2	SC-$SO_2/NO_2/NH_3$
	$1.31\times10^6\pm2.86\times10^4$ (pH>4.1)	$1.63\times10^6\pm2.29\times10^5$ (pH>5.3)	$1.56\times10^8\pm4.67\times10^6$ (pH~0.5)	$5.98\times10^8\pm5.44\times10^6$ (pH~1.6)
Lee and Schwartz, 1983	1.40×10^5 (pH<5.0)	2.00×10^6 (pH>5.8)		
Clifton et al., 1988	1.24×10^7 (pH=5.3)	1.67×10^7 (pH=8.7)		

respectively), indicating that the aerosol water was increased in the presence of NH_3 (Chu et al., 2016). The reaction rate constants between NO_2 and S(IV) in the experiments GR-$SO_2/NO_2/NH_3$(aq) and SC-$SO_2/NO_2/NH_3$ were calculated to be $1.63\times10^6\pm2.29\times10^5\ M^{-1}\ s^{-1}$ and $5.98\times10^8\pm5.44\times10^6\ M^{-1}\ s^{-1}$, respectively. These values are 1.2-fold and 3.8-fold those in the experiments GR-SO_2/NO_2 ($1.31\times10^6\pm2.86\times10^4 M^{-1}\ s^{-1}$) and SC-$SO_2/NO_2$ ($1.56\times10^8\pm4.67\times10^6\ M^{-1}\ s^{-1}$), respectively, indicating an important role of NH_3 in accelerating the aqueous-phase oxidation of SO_2 by NO_2.

As shown in Fig. 1, SO_4^{2-} formation in the aqueous phase is dependent on solubility of SO_2 and NO_2 (process I and II) and aqueous-phase oxidation (process III). Therefore, the increased ratio of SO_4^{2-} concentration ($R[SO_4^{2-}]$) should be equal to the increase ratio of SO_2 dissolution (R[S(IV)]) multiplied by the increase ratio of NO_2 dissolution ($R[NO_2(aq)]$), then multiplied by the increase ratio of the reaction rate constant (R_k), i.e., $R[SO_4^{2-}] = R[S(IV)] \times R[NO_2(aq)] \times R_k$. Gas-phase NH_3 increases all these processes mentioned in Fig. 1, leading to increased SO_4^{2-} formation. The effects of NH_3 on the three processes were evaluated separately in this study. First, the influence of NH_3 on the dissolution of SO_2 was studied in the experiments GR-SO_2/H_2O_2(aq) and GR-$SO_2/NH_3/H_2O_2$(aq) (SI, Table S1). Considering that the reaction rate constant between SO_2 and H_2O_2 ($k = 7.45\times10^7\ M^{-1}\ s^{-1}$) is constant when the solution pH is > 2.5 (Seinfeld and Pandis, 2016), the increased SO_4^{2-} formation in the experiment GR-$SO_2/NH_3/H_2O_2$(aq) compared with that in GR-SO_2/H_2O_2(aq) can be attributed to the increased solubility of SO_2 in the presence of NH_3. Based on the production of SO_4^{2-}, we estimated that SO_2 dissolution was increased by a factor of 3.2 with the coexistence of NH_3. This factor was assumed to be similar in the experiment GR-$SO_2/NO_2/NH_3$(aq) compared to GR-SO_2/NO_2. Similarly, we compared the concentration of nitrate in the experiments GR-$SO_2/NO_2/NH_3$(aq) and GR-SO_2/NO_2, and estimated that NO_2 dissolution was increased by a factor of 1.5 in the presence

of NH_3. These two ratios in processes I and II could not fully explain the 5.3-fold higher SO_4^{2-} formation in the experiment GR-SO_2/NO_2/NH_3(aq) compared to GR-SO_2/NO_2. The remaining increase was attributed to the promotion of the oxidation rate constant, namely process III in Fig. 1. An increase of 12% in the oxidation rate constant with the coexistence of NH_3 was needed to match the total increase of SO_4^{2-} formation. This slight increase in the oxidation rate constant might be attributed to the change in the pH of the aqueous solution. In summary, our estimation showed that the enhancement effects of NH_3 on the solubility of SO_2 and NO_2 were the main factors in promoting SO_4^{2-} formation in the aqueous-phase reaction.

3.4. Influence of ionic strength on aqueous-phase reactions

The electrolyte (i.e., hygroscopic oxalic acid) concentrations were higher in the aerosols in the SC experiments than those in the solution in the GR experiments. Previous studies have shown that electrolyte concentrations can alter the rate constant for a reaction involving a neutral species (e.g., the reactions of nitrogen trioxide (NO_3)) by about one order of magnitude (Herrmann and Zellner, 1998). For the H-abstraction reactions of chlorine radical anion (Cl_2^-) with formaldehyde and formic acid, higher rate constants were observed with increasing ionic strength (Jacobi et al., 1999). Therefore, it is reasonable to attribute the higher reaction rate constant derived from the SC experiments compared to that from the GR experiments to the higher ionic strength (Herrmann et al., 2015) in the aerosol water, where the products and pre-existing electrolyte were highly concentrated.

The ionic strength (I) of a solution is defined as:

$$I = \frac{1}{2}\sum_{i=1}^{n} c_i z_i^2 \quad (8)$$

where c_i is the concentration of species i and Z_i is the ionic charge of species i in aqueous solution.

For a reaction A + B → [A-B]$^{※}$ → P, where reactants A and B form an intermediate product [A-B]*, which then quickly converts into the final product P, the relationship between reaction rate constant (k) and ionic strength (I) can be described by the following equation (Herrmann, 2003):

$$\log\frac{k}{k(I=0)} = \log\gamma_A + \log\gamma_B - \log\gamma_{(AB)} \quad (9)$$

where γ_i is the activity coefficient of species i, and $k(I=0)$ is the kinetic rate constant at the infinite dilution condition, namely $I = 0$ M.

According to the previous reported mechanisms for the reaction of NO_2 with S(IV) (Clifton et al., 1988; Huie, 1994; Nash, 1979; Spindler et al., 2003), the rate-controlling step of this oxidation process involves an ion (i.e., HSO_3^-, SO_3^{2-}) reacting with a neutral molecule (i.e., NO_2). For the neutral species, the expression for the activity coefficient γ_i can be described by equation (10), which indicates that γ_i of the neutral species could be positively influenced by I via the ion-pair interaction (Herrmann, 2003).

$$\log\gamma_i = bI \quad (10)$$

where b is the kinetic salting coefficient.

As a result, the relationship between k and I for the reaction of NO_2 with S(IV) should be expressed as:

$$\log\frac{k}{k(I=0)} = BI \quad (11)$$

In the light of previous studies (Kameoka and Pigford, 1977), B should be a positive value. Therefore, the reaction rate constant k increases with increases in the ionic strength I of the solution.

Based on the concentrations of water-soluble ions (mainly SO_4^{2-}, NO_3^-, NH_4^+) (SI, Table S2), the ionic strength of the reaction systems was low ($I = 2.40 \times 10^{-6}$ M and 7.20×10^{-6} M for GR-SO_2/NO_2 and GR-SO_2/NO_2/NH_3(aq), respectively) in the GR experiments. In a previous study conducted by Lee et al. (Lee and Schwartz, 1983), the initial reaction solution concentration ($[HSO_3^-]_0 = 1.3 \times 10^{-6}$ M) was also low. Hence, it is reasonable that the reaction rate constants derived from the GR experiments in our study are comparable to the results by Lee et al. (Lee and Schwartz, 1983). On the other hand, under a higher S(IV) concentration ($[S(IV)] = 5 \times 10^{-4}$–$2 \times 10^{-3}$ M) condition, Clifton et al. (1988) derived higher rate constants compared to Lee et al. (Lee and Schwartz, 1983) and this study (Table 2). The comparison suggests that higher concentrations of solutes, namely higher ionic strengths in the solution can result in higher rate constants. To test this hypothesis, we performed experiments on the oxidation of SO_2 by NO_2 in solutions with different concentrations of oxalic acid (Table S1). Higher SO_4^{2-} concentrations (Table S2), resulting from higher formation rate constants, were indeed observed for higher concentrations of oxalic acid in solution. A linear relationship between log$k$ and I ($R^2 = 0.99$, blue solid line, Fig. 4) was obtained, which is consistent with equation (11) and thus confirms the hypothesis.

Meanwhile, for the SC experiments SC-SO_2/NO_2 and SC-SO_2/NO_2/NH_3, the oxalic acid seeds were deliquescent under the experimental conditions of RH = (98 ± 1.5) % (Peng et al., 2001), providing an aerosol water reaction medium in which the reactions occurred. Using similar methods as in Guo et al. (2015) (SI, Section S3), the volume of aerosol water was estimated, allowing the concentrations of water-soluble ions (mainly $HC_2O_4^-$, SO_4^{2-}, NO_3^-, and NH_4^+) in this aerosol water (SI, Table S3) and the ionic strength of the solution to be calculated. The ionic strength was much higher ($I = 3.29 \times 10^{-1}$ M and 1.14 M for the experiments SC-SO_2/NO_2 and SC-SO_2/NO_2/NH_3, respectively) in the SC experiments than that in the GR experiments. The higher ionic strengths can explain the high reaction rate constants for SO_4^{2-} formation in the aerosol water. Together with the GR experiments with further reduced ionic strength (i.e., in total 5 experimental data points), an empirical

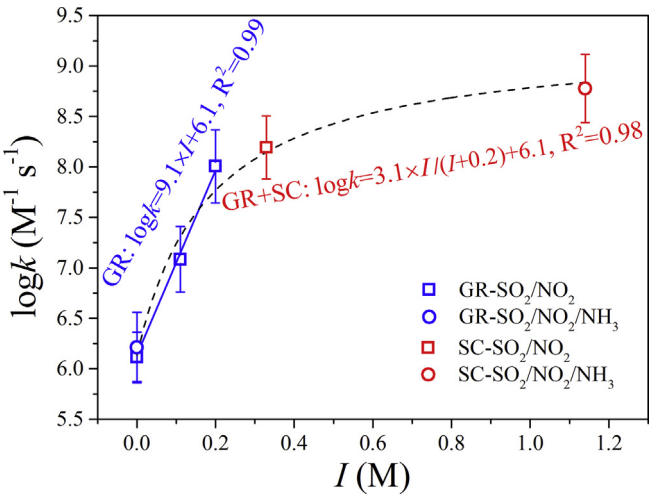

Fig. 4. Relationship between reaction rate constant (k) and ionic strength (I). Each data point refers to an experiment listed in Table 1 and Table S1, and the log$k$-I data corresponding to the all points are given in Table S4. An linear relationship log$k$ = 9.1 × I+6.1 was obtained for GR experiments, while an empirical relationship log$k$ = 3.1 × I/(I+0.2)+6.1 was obtained when combining GR and SC experiments.

relationship between log$k$ and I could also be obtained ($R^2 = 0.98$, black dashed line, Fig. 4). According to this empirical relationship, the reaction rate constant may increase linearly with the increase of ionic strength in aerosol water, but the increase progressively diminish. Although there is no scientific explanation for this phenomenon yet, it is supported by previous studies investigating the salt effect in reactions between ions and dipolar molecules (Amis and Jaffe, 1942; Castanedaagullo et al., 1961). These empirical relationships in Fig. 4 might provide a parameterized solution to the air quality models for simulation of SO_4^{2-} formation in cloud/fog droplets and aerosol water.

4. Conclusions and atmospheric implications

As the major inorganic constituent of atmospheric particle matter (PM), SO_4^{2-} plays an important role in haze pollution not only over North China (Guo et al., 2014; Sun et al., 2016), but also other rapidly developing countries (Gordon, 2003). Based on the present understanding of SO_4^{2-} formation mechanisms, the observed SO_4^{2-} levels cannot be accurately simulated in air quality models, which indicates the presence of reactions and factors in addition to the current formation mechanisms (Gao et al., 2016a; Zheng et al., 2015a). In the present study, the chemical reaction kinetics of aqueous oxidation of SO_2 by NO_2 under different atmospheric conditions were quantitatively evaluated. The GR experimental results, in which we found that SO_2 oxidation by NO_2 contributed significantly to SO_4^{2-} formation, may be applicable to SO_4^{2-} formation in fog and clouds. Meanwhile, the coexistence of NH_3 would mainly enhance the dissolution of SO_2 and NO_2 and subsequently promote SO_4^{2-} formation. The SC experimental results may be applied to SO_4^{2-} formation in aerosol water. Unexpectedly high reaction rate constants for the oxidation of S(IV) by NO_2 were observed in aerosol water, which was attributed to the high ionic strength in the aerosol water.

In severe haze episodes (Gao et al., 2016b), ground-level photochemical reactivity can be weak due to radiative attenuation and the ozone concentration can be low (Zheng et al., 2015b). Gas-phase oxidation of SO_2 by OH and aqueous-phase oxidation of dissolved SO_2 by O_3 and H_2O_2 can be suppressed to a great extent because of the low oxidant levels. Under these situations, the oxidation of S(IV) by NO_2 in the liquid phase may become an essential pathway of SO_4^{2-} formation when RH, NO_2 and NH_3 levels are all high. Such conditions exist in the winter season in cities such as Beijing (Zhang et al., 2015a) and Shanghai (Ye et al., 2011), China, where haze episodes were frequently observed but oxidant levels represented by O_3 were low, yet SO_4^{2-} was high (He et al., 2014; Wang et al., 2016). Using observed NO_2, NH_3 and PM concentrations in such haze episodes (Cheng et al., 2016), the atmospheric lifetime of SO_2 due to oxidation by NO_2 in aerosol water is estimated to be approximately 24 h based on the present laboratory study results (SI, Section S4), which is shorter by an average factor of about 2 than the atmospheric lifetime of SO_2 due to OH oxidation by assuming an daytime average OH concentration of 5.2×10^6 molecules cm^{-3} (Lu et al., 2013). Atmospheric OH concentrations varied a lot ($<1 \times 10^6$–1.7×10^7 molecules cm^{-3}) in different seasons and at different altitudes and latitudes (Lu et al., 2013; Seinfeld and Pandis, 2016; Wang et al., 2016; Yang et al., 2017), while ranged from 2.4×10^6 molecules cm^{-3} to 3.6×10^6 molecules cm^{-3} in Beijing winter (Tan et al., 2018). The atmospheric lifetime of SO_2 due to OH oxidation will increase with decreasing OH concentration in winter time during haze episodes. These SO_2 lifetime analyses suggest that heterogeneous oxidation of SO_2 by NO_2 in aerosol water, especially with the coexistence of NH_3, high concentrations of PM and high RH, is a major pathway for SO_4^{2-} formation in the atmosphere in severe haze episodes. Such a high oxidation rate was clearly promoted by high ionic strengths in aerosol water. High aerosol ionic strengths have been observed in typical haze events in Beijing (Guo et al., 2017), at 12 times higher than that under our experimental conditions. Given the finding of the already large impact under the ionic strength conditions of our laboratory study, the impact of I under real-world haze conditions should be even stronger, and hence should be considered in air quality models to improve simulations of haze formation process.

There have been questions about the importance of the oxidation of SO_2 to SO_4^{2-} by NO_2 based on low pH value predictions for aerosols (Cheng et al., 2016; Guo et al., 2017; Liu et al., 2017; Song et al., 2018; Wang et al., 2018; Wang et al., 2016). Our results indicated that SO_4^{2-} formation by NO_2 oxidation can still be significant in acidic aerosol water under high ionic strength conditions (Table 2). Expanding and continuing the present work to include more atmospherically relevant conditions may provide more accurate kinetic parameters for simulation of SO_4^{2-} formation in air quality models.

Competing financial interests

The authors declare no competing financial interest.

Acknowledgments

This work was supported by the National Key R&D Program of China (2016YFC0202700), National research program for key issues in air pollution control (DQGG0103), the National Natural Science Foundation of China (41877304), the Young Talent Project of the Center for Excellence in Regional Atmospheric Environment, CAS (CERAE201801), Strategic Priority Research Program of the Chinese Academy of Sciences (XDB05010300), the Youth Innovation Promotion Association, CAS (2018060), and Key Research Program of Frontier Sciences, CAS (QYZDB-SSW-DQC018).

Appendix A. Supplementary data

Supplementary data to this article can be found online at https://doi.org/10.1016/j.envpol.2019.05.119.

References

Ali, H.M., Iedema, M., Yu, X.Y., Cowin, J.P., 2014. Ionic strength dependence of the oxidation of SO_2 by H_2O_2 in sodium chloride particles. Atmos. Environ. 89, 731–738.

Amis, E.S., Jaffe, G., 1942. The derivation of a general kinetic equation for reaction between ions and dipolar molecules. J. Chem. Phys. 10, 598–604.

Castanedaagullo, M., Tappel, A.L., Delcastillo, L.M., Whitaker, J.R., 1961. Effect of ionic steength on kinetics of trypsin and alpha chymotrypsin. J. Gen. Physiol. 44, 1103–1120.

Cheng, Y., Zheng, G., Wei, C., Mu, Q., Zheng, B., Wang, Z., Gao, M., Zhang, Q., He, K., Carmichael, G., Pöschl, U., Su, H., 2016. Reactive nitrogen chemistry in aerosol water as a source of sulfate during haze events in China. Sci. Adv. 2, e1601530.

Chu, B., Zhang, X., Liu, Y., He, H., Sun, Y., Jiang, J., Li, J., Hao, J., 2016. Synergetic formation of secondary inorganic and organic aerosol: effect of SO_2 and NH_3 on particle formation and growth. Atmos. Chem. Phys. 16, 14219–14230.

Clegg, S.L., Brimblecombe, P., Wexler, A.S., 1998. Thermodynamic model of the system H^+–NH_4^+–SO_4^{2-}–NO_3^-–H_2O at tropospheric temperatures. J. Phys. Chem. A 102, 2137–2154.

Clifton, C.L., Altstein, N., Huie, R.E., 1988. Rate constant for the reaction of nitrogen dioxide with sulfur(IV) over the pH range 5.3-13. Environ. Sci. Technol. 22, 586–589.

Fedorova, N., Levit, V., da Silva, A.O., dos Santos, D.M.B., 2013. Low visibility formation and forecasting on the northern coast of Brazil. Pure Appl. Geophys. 170, 689–709.

Fu, X., Wang, S.X., Ran, L.M., Pleim, J.E., Cooter, E., Bash, J.O., Benson, V., Hao, J.M., 2015. Estimating NH_3 emissions from agricultural fertilizer application in China using the bi-directional CMAQ model coupled to an agro-ecosystem model. Atmos. Chem. Phys. 15, 6637–6649.

Gao, M., Carmichael, G.R., Wang, Y., Ji, D., Liu, Z., Wang, Z., 2016a. Improving simulations of sulfate aerosols during winter haze over Northern China: the impacts of heterogeneous oxidation by NO_2. Front. Environ. Sci. Eng. 10, 16.

Gao, M., Carmichael, G.R., Wang, Y., Saide, P.E., Yu, M., Xin, J., Liu, Z., Wang, Z., 2016b. Modeling study of the 2010 regional haze event in the North China Plain. Atmos. Chem. Phys. 16, 1673–1691.
Gordon, M.M.F., 2003. Air pollution and health in rapidly developing countries. Manag. Environ. Qual. Int. J. 14, 542–543.
Guo, H., Weber, R.J., Nenes, A., 2017. High levels of ammonia do not raise fine particle pH sufficiently to yield nitrogen oxide-dominated sulfate production. Sci. Rep. 7, 12109.
Guo, H., Xu, L., Bougiatioti, A., Cerully, K.M., Capps, S.L., Hite Jr., J.R., Carlton, A.G., Lee, S.H., Bergin, M.H., Ng, N.L., Nenes, A., Weber, R.J., 2015. Fine-particle water and pH in the southeastern United States. Atmos. Chem. Phys. 15, 5211–5228.
Guo, S., Hu, M., Zamora, M.L., Peng, J., Shang, D., Zheng, J., Du, Z., Wu, Z., Shao, M., Zeng, L., Molina, M.J., Zhang, R., 2014. Elucidating severe urban haze formation in China. Proc. Natl. Acad. Sci. U.S.A. 111, 17373–17378.
He, H., Wang, Y., Ma, Q., Ma, J., Chu, B., Ji, D., Tang, G., Liu, C., Zhang, H., Hao, J., 2014. Mineral dust and NO_x promote the conversion of SO_2 to sulfate in heavy pollution days. Sci. Rep. 4, 4172.
He, K., Yang, F., Ma, Y., Zhang, Q., Yao, X., Chan, C.K., Cadle, S., Chan, T., Mulawa, P., 2001. The characteristics of $PM_{2.5}$ in Beijing, China. Atmos. Environ. Times 35, 4959–4970.
Herrmann, H., 2003. Kinetics of aqueous phase reactions relevant for atmospheric chemistry. Chem. Rev. 103, 4691–4716.
Herrmann, H., Schaefer, T., Tilgner, A., Styler, S.A., Weller, C., Teich, M., Otto, T., 2015. Tropospheric aqueous-phase chemistry: kinetics, mechanisms, and its coupling to a changing gas phase. Chem. Rev. 115, 4259–4334.
Herrmann, H., Zellner, R., 1998. Reactions of NO_3-radicals in aqueous solution. In: Alfassi, Z.B. (Ed.), N-centered Radicals. John Wiley, New York, pp. 291–343.
Hu, G., Sun, Z., Gao, H., 2010. Novel process of simultaneous removal of SO_2 and NO_2 by sodium humate solution. Environ. Sci. Technol. 44, 6712–6717.
Huie, R.E., 1994. The reaction kinetics of NO_2. Toxicology 89, 193–216.
Huie, R.E., Neta, P., 1986. Kinetics of one-electron transfer reactions involving chlorine dioxide and nitrogen dioxide. J. Phys. Chem. 90, 1193–1198.
Hung, H.-M., Hoffmann, M.R., 2015. Oxidation of gas-phase SO_2 on the surfaces of acidic microdroplets: implications for sulfate and sulfate radical anion formation in the atmospheric liquid phase. Environ. Sci. Technol. 49, 13768–13776.
Ianniello, A., Spataro, F., Esposito, G., Allegrini, I., Rantica, E., Ancora, M.P., Hu, M., Zhu, T., 2010. Occurrence of gas phase ammonia in the area of Beijing (China). Atmos. Chem. Phys. 10, 9487–9503.
Jacob, D.J., 2000. Heterogeneous chemistry and tropospheric ozone. Atmos. Environ. 34, 2131–2159.
Jacobi, H.W., Wicktor, F., Herrmann, H., Zellner, R., 1999. A laser flash photolysis kinetic study of reactions of the Cl_2^- radical anion with oxygenated hydrocarbons in aqueous solution. Int. J. Chem. Kinet. 31, 169–181.
Jia, S., Wang, X., Zhang, Q., Sarkar, S., Wu, L., Huang, M., Zhang, J., Yang, L., 2018. Technical note: comparison and interconversion of pH based on different standard states for aerosol acidity characterization. Atmos. Chem. Phys. 18, 11125–11133.
Kameoka, Y., Pigford, R.L., 1977. Absorption of nitrogen dioxide into water, sulfuric acid, sodium hydroxide, and alkaline sodium sulfite aqueous solutions. Ind. Eng. Chem. Fundam. 16, 163–169.
Kong, L.D., Zhao, X., Sun, Z.Y., Yang, Y.W., Fu, H.B., Zhang, S.C., Cheng, T.T., Yang, X., Wang, L., Chen, J.M., 2014. The effects of nitrate on the heterogeneous uptake of sulfur dioxide on hematite. Atmos. Chem. Phys. 14, 9451–9467.
Lee, Y.N., Schwartz, S.E., 1983. Kinetics of oxidation of aqueous sulfur (IV) by nitrogen dioxide. In: Pruppacher, H.R., Semonin, R.G., Slinn, W.G.N. (Eds.), Precipitation Scavenging, Dry Deposition and Resuspension. Elsevier, New York, pp. 453–466.
Li, G., Bei, N., Cao, J., Huang, R., Wu, J., Feng, T., Wang, Y., Liu, S., Zhang, Q., Tie, X., Molina, L.T., 2017a. A possible pathway for rapid growth of sulfate during haze days in China. Atmos. Chem. Phys. 17, 3301–3316.
Li, L., Hoffmann, M.R., Colussi, A.J., 2018. Role of nitrogen dioxide in the production of sulfate during Chinese Haze-Aerosol Episodes. Environ. Sci. Technol. 52, 2686–2693.
Li, L., Tan, Q., Zhang, Y., Feng, M., Qu, Y., An, J., Liu, X., 2017b. Characteristics and source apportionment of $PM_{2.5}$ during persistent extreme haze events in Chengdu, southwest China. Environ. Pollut. 230, 718–729.
Littlejohn, D., Wang, Y., Chang, S.G., 1993. Oxidation of aqueous sulfite ion by nitrogen dioxide. Environ. Sci. Technol. 27, 2162–2167.
Liu, C., Ma, Q., Liu, Y., Ma, J., He, H., 2012. Synergistic reaction between SO_2 and NO_2 on mineral oxides: a potential formation pathway of sulfate aerosol. Phys. Chem. Chem. Phys. 14, 1668–1676.
Liu, M., Song, Y., Zhou, T., Xu, Z., Yan, C., Zheng, M., Wu, Z., Hu, M., Wu, Y., Zhu, T., 2017. Fine particle pH during severe haze episodes in northern China. Geophys. Res. Lett. 44, 5213–5221.
Liu, X.G., Li, J., Qu, Y., Han, T., Hou, L., Gu, J., Chen, C., Yang, Y., Liu, X., Yang, T., Zhang, Y., Tian, H., Hu, M., 2013. Formation and evolution mechanism of regional haze: a case study in the megacity Beijing, China. Atmos. Chem. Phys. 13, 4501–4514.
Lu, K.D., Hofzumahaus, A., Holland, F., Bohn, B., Brauers, T., Fuchs, H., Hu, M., Häseler, R., Kita, K., Kondo, Y., Li, X., Lou, S.R., Oebel, A., Shao, M., Zeng, L.M., Wahner, A., Zhu, T., Zhang, Y.H., Rohrer, F., 2013. Missing OH source in a suburban environment near Beijing: observed and modelled OH and HO_2 concentrations in summer 2006. Atmos. Chem. Phys. 13, 1057–1080.
Ma, Q., Liu, Y., He, H., 2008. Synergistic effect between NO_2 and SO_2 in their adsorption and reaction on γ-alumina. J. Phys. Chem. A 112, 6630–6635.
Maahs, H.G., 1983. Kinetics and mechanism of the oxidation of S(IV) by ozone in aqueous solution with particular reference to SO_2 conversion in nonurban tropospheric clouds. J. Geophys. Res. Atmos. 88, 10721–10732.
Maaß, F., Elias, H., Wannowius, K.J., 1999. Kinetics of the oxidation of hydrogen sulfite by hydrogen peroxide in aqueous solution: ionic strength effects and temperature dependence. Atmos. Environ. 33, 4413–4419.
Mauldin Iii, R.L., Berndt, T., Sipilä, M., Paasonen, P., Petäjä, T., Kim, S., Kurtén, T., Stratmann, F., Kerminen, V.M., Kulmala, M., 2012. A new atmospherically relevant oxidant of sulphur dioxide. Nature 488, 193.
McVay, R., Ervens, B., 2017. A microphysical parameterization of aqSOA and sulfate formation in clouds. Geophys. Res. Lett. 44, 7500–7509.
Meng, Z.Y., Lin, W.L., Jiang, X.M., Yan, P., Wang, Y., Zhang, Y.M., Jia, X.F., Yu, X.L., 2011. Characteristics of atmospheric ammonia over Beijing, China. Atmos. Chem. Phys. 11, 6139–6151.
Nash, T., 1979. The effect of nitrogen dioxide and of some transition metals on the oxidation of dilute bisulphite solutions. Atmos. Environ. 13, 1149–1154.
Pachauri, T., Singla, V., Satsangi, A., Lakhani, A., Kumari, K.M., 2013. Characterization of major pollution events (dust, haze, and two festival events) at Agra, India. Environ. Sci. Pollut. Res. 20, 5737–5752.
Pathak, R.K., Wu, W.S., Wang, T., 2009. Summertime $PM_{2.5}$ ionic species in four major cities of China: nitrate formation in an ammonia-deficient atmosphere. Atmos. Chem. Phys. 9, 1711–1722.
Peng, C., Chan, M.N., Chan, C.K., 2001. The hygroscopic properties of dicarboxylic and multifunctional acids: measurements and UNIFAC predictions. Environ. Sci. Technol. 35, 4495–4501.
Pye, H.O.T., Zuend, A., Fry, J.L., Isaacman-VanWertz, G., Capps, S.L., Appel, K.W., Foroutan, H., Xu, L., Ng, N.L., Goldstein, A.H., 2018. Coupling of organic and inorganic aerosol systems and the effect on gas–particle partitioning in the southeastern US. Atmos. Chem. Phys. 18, 357–370.
Quan, J., Liu, Q., Li, X., Gao, Y., Jia, X., Sheng, J., Liu, Y., 2015. Effect of heterogeneous aqueous reactions on the secondary formation of inorganic aerosols during haze events. Atmos. Environ. 122, 306–312.
Seinfeld, J.H., Pandis, S.N., 2016. Atmospheric Chemistry and Physics: from Air Pollution to Climate Change. John Wiley & Sons, Hoboken, NJ.
Shen, C.H., Rochelle, G.T., 1998. Nitrogen dioxide absorption and sulfite oxidation in aqueous sulfite. Environ. Sci. Technol. 32, 1994–2003.
Shen, X.J., Sun, J.Y., Zhang, X.Y., Zhang, Y.M., Zhang, L., Che, H.C., Ma, Q.L., Yu, X.M., Yue, Y., Zhang, Y.W., 2015. Characterization of submicron aerosols and effect on visibility during a severe haze-fog episode in Yangtze River Delta, China. Atmos. Environ. 120, 307–316.
Song, S., Gao, M., Xu, W., Shao, J., Shi, G., Wang, S., Wang, Y., Sun, Y., McElroy, M.B., 2018. Fine-particle pH for Beijing winter haze as inferred from different thermodynamic equilibrium models. Atmos. Chem. Phys. 18, 7423–7438.
Spindler, G., Hesper, J., Brüggemann, E., Dubois, R., Müller, T., Herrmann, H., 2003. Wet annular denuder measurements of nitrous acid: laboratory study of the artefact reaction of NO_2 with S(IV) in aqueous solution and comparison with field measurements. Atmos. Environ. 37, 2643–2662.
Sun, Y., Chen, C., Zhang, Y., Xu, W., Zhou, L., Cheng, X., Zheng, H., Ji, D., Li, J., Tang, X., Fu, P., Wang, Z., 2016. Rapid formation and evolution of an extreme haze episode in Northern China during winter 2015. Sci. Rep. 6, 27151.
Sun, Y., Zhuang, G., Tang, A., Wang, Y., An, Z., 2006. Chemical characteristics of $PM_{2.5}$ and PM_{10} in haze-fog episodes in Beijing. Environ. Sci. Technol. 40, 3148–3155.
Takekawa, H., Minoura, H., Yamazaki, S., 2003. Temperature dependence of secondary organic aerosol formation by photo-oxidation of hydrocarbons. Atmos. Environ. 37, 3413–3424.
Takeuchi, H., Ando, M., Kizawa, N., 1977. Absorption of nitrogen oxides in aqueous sodium sulfite and bisulfite solutions. Ind. Eng. Chem. Process Des. Dev. 16, 303–308.
Tan, J.-H., Duan, J.-C., Chen, D.-H., Wang, X.-H., Guo, S.-J., Bi, X.-H., Sheng, G.-Y., He, K.-B., Fu, J.-M., 2009. Chemical characteristics of haze during summer and winter in Guangzhou. Atmos. Res. 94, 238–245.
Tan, Z., Rohrer, F., Lu, K., Ma, X., Bohn, B., Broch, S., Dong, H., Fuchs, H., Gkatzelis, G.I., Hofzumahaus, A., Holland, F., Li, X., Liu, Y., Liu, Y., Novelli, A., Shao, M., Wang, H., Wu, Y., Zeng, L., Hu, M., Kiendler-Scharr, A., Wahner, A., Zhang, Y., 2018. Wintertime photochemistry in Beijing: observations of RO_x radical concentrations in the North China Plain during the BEST-ONE campaign. Atmos. Chem. Phys. 18, 12391–12411.
Turšič, J., Berner, A., Podkrajšek, B., Grgić, I., 2004. Influence of ammonia on sulfate formation under haze conditions. Atmos. Environ. 38, 2789–2795.
Wang, G., Zhang, F., Peng, J., Duan, L., Ji, Y., Marrero-Ortiz, W., Wang, J., Li, J., Wu, C., Cao, C., Wang, Y., Zheng, J., Secrest, J., Li, Y., Wang, Y., Li, H., Li, N., Zhang, R., 2018. Particle acidity and sulfate production during severe haze events in China cannot be reliably inferred by assuming a mixture of inorganic salts. Atmos. Chem. Phys. 18, 10123–10132.
Wang, G., Zhang, R., Gomez, M.E., Yang, L., Levy Zamora, M., Hu, M., Lin, Y., Peng, J., Guo, S., Meng, J., Li, J., Cheng, C., Hu, T., Ren, Y., Wang, Y., Gao, J., Cao, J., An, Z., Zhou, W., Li, G., Wang, J., Tian, P., Marrero-Ortiz, W., Secrest, J., Du, Z., Zheng, J., Shang, D., Zeng, L., Shao, M., Wang, W., Huang, Y., Wang, Y., Zhu, Y., Li, Y., Hu, J., Pan, B., Cai, L., Cheng, Y., Ji, Y., Zhang, F., Rosenfeld, D., Liss, P.S., Duce, R.A., Kolb, C.E., Molina, M.J., 2016. Persistent sulfate formation from London Fog to Chinese haze. Proc. Natl. Acad. Sci. U.S.A. 113, 13630–13635.
Wang, Y., Zhuang, G., Tang, A., Yuan, H., Sun, Y., Chen, S., Zheng, A., 2005. The ion chemistry and the source of $PM_{2.5}$ aerosol in Beijing. Atmos. Environ. 39, 3771–3784.
Welz, O., Savee, J.D., Osborn, D.L., Vasu, S.S., Percival, C.J., Shallcross, D.E.,

Taatjes, C.A., 2012. Direct kinetic measurements of Criegee Intermediate (CH_2OO) formed by reaction of CH_2I with O_2. Science 335, 204–207.
Wexler, A.S., Clegg, S.L., 2002. Atmospheric aerosol models for systems including the ions H^+, NH_4^+, Na^+, SO_4^{2-}, NO_3^-, Cl^-, Br^-, and H_2O. J. Geophys. Res. Atmos. 107, 4207.
Xie, Y., Ding, A., Nie, W., Mao, H., Qi, X., Huang, X., Xu, Z., Kerminen, V.-M., Petaja, T., Chi, X., Virkkula, A., Boy, M., Xue, L., Guo, J., Sun, J., Yang, X., Kulmala, M., Fu, C., 2015. Enhanced sulfate formation by nitrogen dioxide: implications from in situ observations at the SORPES station. J. Geophys. Res. Atmos. 120, 12679–12694.
Xue, J., Yuan, Z., Griffith, S.M., Yu, X., Lau, A.K.H., Yu, J.Z., 2016. Sulfate formation enhanced by a Cocktail of high NO_x, SO_2, particulate matter, and droplet pH during haze-fog events in megacities in China: an observation-based modeling investigation. Environ. Sci. Technol. 50, 7325–7334.
Yang, F., Tan, J., Zhao, Q., Du, Z., He, K., Ma, Y., Duan, F., Chen, G., Zhao, Q., 2011. Characteristics of $PM_{2.5}$ speciation in representative megacities and across China. Atmos. Chem. Phys. 11, 5207–5219.
Yang, S., Yuesi, W., Changchun, Z., 2009. Measurement of the vertical profile of atmospheric SO_2 during the heating period in Beijing on days of high air pollution. Atmos. Environ. 43, 468–472.
Yang, W., He, H., Ma, Q., Ma, J., Liu, Y., Liu, P., Mu, Y., 2016. Synergistic formation of sulfate and ammonium resulting from reaction between SO_2 and NH_3 on typical mineral dust. Phys. Chem. Chem. Phys. 18, 956–964.
Yang, Y., Shao, M., Keßel, S., Li, Y., Lu, K., Lu, S., Williams, J., Zhang, Y., Zeng, L., Nölscher, A.C., Wu, Y., Wang, X., Zheng, J., 2017. How the OH reactivity affects the ozone production efficiency: case studies in Beijing and Heshan, China. Atmos. Chem. Phys. 17, 7127–7142.
Ye, X., Ma, Z., Zhang, J., Du, H., Chen, J., Chen, H., Yang, X., Gao, W., Geng, F., 2011. Important role of ammonia on haze formation in Shanghai. Environ. Res. Lett. 6, 024019.
Zhang, L., Liu, L., Zhao, Y., Gong, S., Zhang, X., Henze, D.K., Capps, S.L., Fu, T.-M., Zhang, Q., Wang, Y., 2015a. Source attribution of particulate matter pollution over North China with the adjoint method. Environ. Res. Lett. 10, 084011.
Zhang, R., Wang, G., Guo, S., Zamora, M.L., Ying, Q., Lin, Y., Wang, W., Hu, M., Wang, Y., 2015b. Formation of urban fine particulate matter. Chem. Rev. 115, 3803–3855.
Zhang, T., Cao, J.J., Tie, X.X., Shen, Z.X., Liu, S.X., Ding, H., Han, Y.M., Wang, G.H., Ho, K.F., Qiang, J., Li, W.T., 2011. Water-soluble ions in atmospheric aerosols measured in Xi'an, China: seasonal variations and sources. Atmos. Res. 102, 110–119.
Zhao, P.S., Dong, F., He, D., Zhao, X.J., Zhang, X.L., Zhang, W.Z., Yao, Q., Liu, H.Y., 2013. Characteristics of concentrations and chemical compositions for $PM_{2.5}$ in the region of Beijing, Tianjin, and Hebei, China. Atmos. Chem. Phys. 13, 4631–4644.
Zheng, B., Zhang, Q., Zhang, Y., He, K.B., Wang, K., Zheng, G.J., Duan, F.K., Ma, Y.L., Kimoto, T., 2015a. Heterogeneous chemistry: a mechanism missing in current models to explain secondary inorganic aerosol formation during the January 2013 haze episode in North China. Atmos. Chem. Phys. 15, 2031–2049.
Zheng, G.J., Duan, F.K., Su, H., Ma, Y.L., Cheng, Y., Zheng, B., Zhang, Q., Huang, T., Kimoto, T., Chang, D., Pöschl, U., Cheng, Y.F., He, K.B., 2015b. Exploring the severe winter haze in Beijing: the impact of synoptic weather, regional transport and heterogeneous reactions. Atmos. Chem. Phys. 15, 2969–2983.